Title

Size-specific growth and grazing rates for picophytoplankton in coastal and oceanic regions of the eastern Pacific

Authors

Taniguchi, DAA
Landry, MR
Franks, PJS
et al.

Publication Date

2014-08-27

DOI

10.3354/meps10895

Peer reviewed

Vol. 509: 87–101, 2014
doi: 10.3354/meps10895

MARINE ECOLOGY PROGRESS SERIES
Mar Ecol Prog Ser

Published August 27

Size-specific growth and grazing rates for picophytoplankton in coastal and oceanic regions of the eastern Pacific

Darcy A. A. Taniguchi[1,*], Michael R. Landry[1], Peter J. S. Franks[1], Karen E. Selph[2]

[1]Scripps Institution of Oceanography, University of California, San Diego, La Jolla, California 92093, USA
[2]Department of Oceanography, University of Hawaii at Manoa, Honolulu, Hawaii 96822, USA

ABSTRACT: Estimates of growth and grazing mortality rates for different size classes and taxa of natural picophytoplankton assemblages were measured in mixed-layer experiments conducted in 3 regions of the eastern Pacific: the California Current Ecosystem, Costa Rica Dome, and equatorial Pacific. Contrary to expectation, size-dependent rates for cells between 0.45 and 4.0 µm in diameter showed no systematic trends with cell size both in and among regions. For all size classes, mean ± SD growth rates ranged from –0.70 ± 0.17 to 0.83 ± 0.13 d^{-1} and grazing rates between –0.07 ± 0.13 and 1.17 ± 0.10 d^{-1}. Taxon-specific growth rates for *Prochlorococcus* ranged from 0.17 ± 0.12 to 0.59 ± 0.01 d^{-1}, for *Synechococcus* from 0.68 ± 0.03 to 0.97 ± 0.04 d^{-1}, for picoeukaryotes from 0.46 ± 0.13 to 1.03 ± 0.06 d^{-1}, and for all cells combined between 0.45 ± 0.03 and 0.65 ± 0.02 d^{-1}. For grazing, *Prochlorococcus* rates ranged between 0.02 ± 0.12 and 0.66 ± 0.02 d^{-1}, *Synechococcus* rates between 0.24 ± 0.08 and 0.92 ± 0.05 d^{-1}, for picoeukaryotes between 0.19 ± 0.10 and 0.78 ± 0.09 d^{-1}, and for all cells between 0.16 ± 0.05 and 0.75 ± 0.02 d^{-1}. When comparing rates among taxa, only *Prochlorococcus* had consistently lower rates than *Synechococccocus* in all regions. No other trends were apparent. Temperature relationships based on the Metabolic Theory of Ecology were able to explain more of the variability among grazing rates than among growth rates for each taxon considered.

KEY WORDS: Size-specific rates · California Current Ecosystem · Costa Rica Dome · Equatorial Pacific · *Prochlorococcus* · *Synechococcus* · Picoeukaryotes

INTRODUCTION

Planktonic populations show systematic changes in abundance and biomass with size in many regions of the world's oceans (Rodriguez & Mullin 1986, Chisholm 1992, Cavender-Bares et al. 2001, Huete-Ortega et al. 2010). Although community structure is a revealing property of ecosystems, it is the net result of many processes. To understand what leads to observed structure and composition, it is necessary to examine the rates of the underlying processes. For example, phytoplankton growth (Banse 1976, Tang 1995) and grazing rates (Hansen et al. 1997) have been suggested to decrease in general with increasing size, while half-saturation constants for nutrient uptake increase with size (Edwards et al. 2012).

Uncovering the size dependencies of rates can provide useful insight into the processes that regulate planktonic populations. However, the vast majority of rates come from laboratory measurements—although see Chen & Liu (2010), Marañón et al. (2007), Bec et al. (2008), and Huete-Ortega et al. (2012)—and are typically only for monospecific cultures. These laboratory rates may therefore not translate easily to different natural environmental conditions or to mixed plankton assemblages. Furthermore, most syntheses of size-dependent rates are designed to demonstrate trends over several orders of magnitude in size.

Here we take a different approach by examining the growth and grazing mortality rates of naturally occurring picophytoplankton (≤4 µm). We focused on

*Corresponding author: datanigu@mit.edu

this size range for several reasons. These single-celled organisms are the base of ocean food webs, typically the dominant primary producers in open-ocean ecosystems (Raven 1998, Pomeroy et al. 2007). They may even become more important under future climatic conditions, at least in non-light-limited areas where warming-induced stratification decreases nutrient supply (Marañón et al. 2012). It is also only for this smaller end of the phytoplankton size spectrum that one can reasonably argue that the major sources of cell mortality reside at near full strength in easily collected seawater samples, as opposed to larger cells with increasing vulnerabilities to grazing by net-collected zooplankton.

Focusing on the rates of picophytoplankton is also of interest given recent evidence that patterns in their size-dependent rates may differ from the overarching trend found over larger size ranges. That is, while several studies have shown that both growth and grazing rates decrease with size over a broad size range (Tang 1995, Hansen et al. 1997, Edwards et al. 2012), there is growing evidence that picoplanktonic rates may show different patterns. Raven (1994) provides a theoretical basis for increasing growth rates of picoplankton with increasing size. The hypothesis best supported by empirical data is that non-scalable components (e.g. DNA) take up a higher proportion of biomass in small cells compared to large cells, leading to less room for scalable components (e.g. catalysts) essential for growth. Consequently, smaller cells have a lower specific growth rate. Marañón et al. (2013) also showed that phytoplankton growth rates, measured under standardized laboratory conditions, initially increased with size up to ~100 μm^3 biovolume and then declined, similar to the theoretical and experimental work of Kempes et al. (2012). Bec et al. (2008) and Chen & Liu (2010) also found unimodal patterns in field data from a marine lagoon and a compilation of global field data, respectively. However, Huete-Ortega et al. (2012) demonstrated that the metabolism of natural phytoplankton populations in the Atlantic Ocean, measured as the carbon fixation rate per unit volume, varied isometrically with size. There is also evidence that grazing rate varies positively with cell size (Chen & Liu 2010). Clearly, there is substantial uncertainty in our understanding of the size-based scaling of picoplanktonic rates. Some of these discrepancies may arise from a difference in what is measured—namely, rates based strictly on cell size versus rates measured for different taxa that are then ordered by mean size.

In addition to the physiological constraints that size places on maximal growth and grazing rates, realized rates *in situ* are also influenced by environmental factors such as temperature (Eppley & Sloan 1966, Eppley 1972, Caron et al. 2000, Chen et al. 2012), light (Eppley & Sloan 1966, Jassby & Platt 1976), nutrients (Martin & Fitzwater 1988, Elser et al. 1990, Landry et al. 2000, 2008), turbulence (Rothschild & Osborn 1988, Pecseli et al. 2012), species composition (Saito et al. 2006, Sherr & Sherr 2007), or their interactive effects (Eppley 1972, Vidal 1980, Rhee & Gotham 1981, Sunda & Huntsman 1997, Riegman et al. 2000, Litchman et al. 2004, Rose et al. 2009, Lawrence & Menden-Deuer 2012). Estimating *in situ* rates in the context of such environmental variability is critical for understanding how processes actually drive changes in biomass and composition of planktonic assemblages and for representing planktonic ecosystem dynamics accurately in models. Particularly important in the context of future climatic conditions, theoretical evidence from the Metabolic Theory of Ecology (MTE) (Brown et al. 2004) indicates that temperature may affect heterotrophic processes more than autotrophic processes, an idea in alignment with empirical evidence (Rose & Caron 2007, López-Urrutia 2008), but see the Discussion for further details on this topic.

In this study, we examine growth and grazing mortality rates of natural picophytoplankton assemblages collected in 3 regions of the eastern Pacific: the California Current Ecosystem (CCE), the Costa Rica Dome (CRD), and the equatorial Pacific (EP). To estimate these rates, 2-point dilution experiments (Landry et al. 1995b, 2011b), a streamlined version of the traditional dilution method (Landry & Hassett 1982), were conducted after validating the linearity of the net growth response with dilution at each location. While some results from these regions have been described previously (Landry et al. 2009, 2011a, Selph et al. 2011), the present study differs in 3 main respects: (1) we examined size-dependent, non-taxonomic rates over a limited size range of phytoplankton (<4 µm) using the size-dependent dilution method (Taniguchi et al. 2012), (2) we compared these size-dependent rates of mixed assemblages with those of taxonomic-based rates, and (3) we compared patterns, or the lack thereof, across these different regions. By examining growth and grazing rates from these perspectives, we can address whether growth and grazing rates in these areas of the eastern Pacific show a decreasing pattern with increasing size, as is seen over larger size ranges (e.g. Tang 1995, Hansen et al. 1997), the opposite pattern (Chen & Liu 2010, Marañón et al. 2013), or no size-dependent pattern at all (Huete-Ortega et al.

2012). To evaluate the environmental component of rate variability, we tested whether our data correspond with the prediction from MTE that grazing rates vary more with temperature than growth rates.

MATERIALS AND METHODS

Study regions and experiments

The 3 study regions are coastal to open-ocean upwelling systems of the eastern Pacific (Fig. 1). Comparable experimental studies of these regions were conducted during 3 cruises: September 2005 (EP), May and June 2006 (CCE), and July 2010 (CRD).

Equatorial Pacific

The EP is a major high-nitrate low-chlorophyll (HNLC) region where active upwelling divergence along the equator brings deeper, nutrient-rich water to the surface (Barber et al. 1996). Despite high macronutrient concentrations, low phytoplankton biomass prevails due to limitation by the micronutrient iron (Coale et al. 1996). Microzooplankton grazing has also been demonstrated to be important in controlling picophytoplankton populations in the EP in response to natural variability and experimental additions of iron (Landry et al. 1997, 2000).

The EP region was sampled on the Equatorial Biocomplexity cruise EB05 (Nelson & Landry 2011) along a zonal transect at 0.5° N, with one station at 140° W and the other 5 stations approximately 2° apart between 132.5 and 123.5° W (Landry et al. 2011a) (Fig. 1). Sampling of 8 other stations was also conducted along a meridional transect at 140° W between 4° N and 2.5° S.

The experimental approach is described briefly here and more fully elsewhere (Landry et al. 2011a, Selph et al. 2011). Sampling was conducted at 8 depths from the surface to the base of the euphotic zone in early morning CTD casts (~03:00 to 04:00 h local time), which were also used to collect standard hydrographic data including temperature, salinity, and micronutrients. To eliminate confounding problems with vertical light gradients, here we use only experiments conducted with mixed-layer water at 50 and 31% of surface irradiance. Given the similar rates found at these 2 light levels (Landry et al. 2011a, Selph et al. 2011), we combined samples from these depths to decrease error in the rate estimates

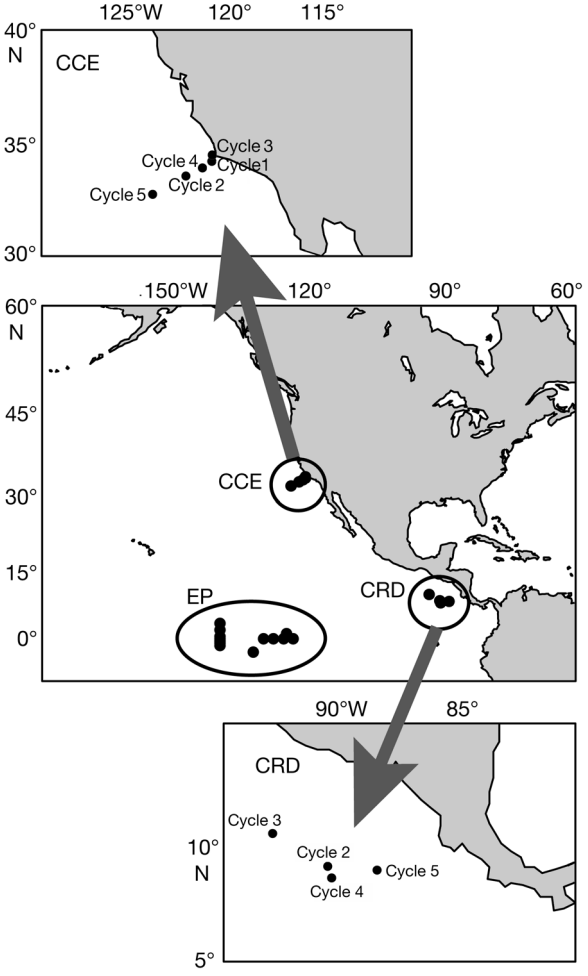

Fig. 1. Map of study regions. The black dots represent sampling stations in the equatorial Pacific (EP) and the beginning location of each experimental cycle in the California Current Ecosystem (CCE) and Costa Rica Dome (CRD). The insets are enlargements of the CCE and CRD

(Taniguchi et al. 2012). For our 2-point dilution experiments, dilution treatments (fraction of unfiltered seawater $d = 1$ and $d \approx 0.37$) were prepared in 2.8 l polycarbonate bottles. The unfiltered seawater came, via silicone tubing, directly from Niskin bottles attached to the CTD rosette. The filtered seawater also came from the Niskin bottles but was filtered using silicone tubing and a peristaltic pump through a 0.1 µm Suporcap filter capsule that had been prewashed with 10% trace-metal grade HCl and rinsed with Milli-Q water and seawater. The treatments were incubated for 24 h in light-calibrated seawater-cooled deck incubators, screened with plastic film to correspond to light at the depth from which the samples were taken. The filled incubators were calibrated on site to incident PAR with a Biospherical

QSL-100 Quantum Scalar Irradiance Meter. Flow cytometry (FCM) samples (2 ml, 0.5% v/v paraformaldehyde preserved, frozen in liquid nitrogen) were taken from both treatment bottles at the beginning and end of each incubation.

California Current Ecosystem

The CCE off the coast of the western United States and Baja California is the eastern boundary current at the eastern edge of the anticyclonic North Pacific Subtropical Gyre (Lynn & Simpson 1987). The CCE is a coastal upwelling area, with alongshore upwelling-favorable winds reaching highest velocities during the spring and summer (Hickey 1979). Adjacent to the coast, winds force surface waters offshore, leading to substantial input of nutrient-rich waters from depth in the nearshore environment. Nutrients also enter the system through the spatial gradient in winds, called wind-stress curl, which moves deep water toward the surface at a slower rate but over a much wider area than coastal upwelling (Rykaczewski & Checkley 2008).

The CCE dilution experiments were conducted on process cruise P0605 of the CCE-LTER (Long Term Ecological Research) Program in May and June 2006 (Landry et al. 2009), which are months of strong upwelling in the region. Sampling and experimentation occurred in 5 water parcels that were tracked via a satellite-equipped drift array off Point Conception, California (Fig. 1). The drift array was a World Ocean Circulation Experiment, Surface Velocity Program design and contained a strobe light and Globalstar telemetry that transmitted its position every 30 min. The drift array served as a platform for incubation experiments and included a holey sock drogue at ~15 m that allowed for quasi-Lagrangian tracking of each water parcel for 3 to 5 d 'cycles', during which ecosystem variables and processes were experimentally studied as they evolved. These experimental cycles were chosen specifically to span the environmental variability that exists spatially in this region and were identified using satellite imagery of chlorophyll *a* (chl *a*) and temperature along with subsurface conditions from Spray ocean gliders. Experimental Cycles 1 and 3 were inshore, and Cycles 2 and 5 were offshore (Fig. 1). Cycle 4 was nutrient-depleted coastal water that had been advected offshore.

Seawater for the 2-point dilution experiments was collected at 8 different depths, but here, again, we focus on water from the surface mixed layer, between ~5 and 12 m. Similar to the samples from the EP region, the seawater was collected from Niskin bottles at the specified depths. The whole seawater was added to the experimental 2.8 l polycarbonate bottles via silicone tubing. The filtered seawater was passed through a 0.1 µm Suporcap filter capsule that had been washed with 10% trace-metal grade HCl and subsequently rinsed with Milli-Q water and seawater. The diluted treatment contained ~1/3 the amount of unfiltered seawater as the undiluted treatment. Both treatments were placed in 2.8 l polycarbonate bottles and incubated for 24 h *in situ* in mesh bags on the drift array at the depth from which the samples were taken (Landry et al. 2009). Initial and final FCM samples (2 ml) were taken from diluted and undiluted treatments and preserved as above for the EP.

Costa Rica Dome

The CRD is an open-ocean upwelling region in the eastern tropical Pacific with a mean location of approximately 9° N, 90° W (Fiedler 2002) (Fig. 1). Originally described as being caused by opposing currents in the region (Wyrtki 1964), the CRD has since been shown to develop from local wind stress curl (Hofmann et al. 1981, Fiedler 2002) or in response to tradewinds coming together at the intertropical convergence zone (Umatani & Yamagata 1991). The magnitude of upwelling and location of the dome varies seasonally, with the thermocline initially shoaling near the coast in February to April before moving offshore and deepening later in the year (Fiedler 2002).

Dilution experiments from the CRD were conducted in July 2010 as part of the CRD Flux and Zinc Experiments (FLUZiE) cruise. Similar to the CCE, samples were collected from spatially separated water parcels tracked for 4 d cycles by satellite-tracked drift arrays with mixed-layer drogues. Here we focus only on Cycles 2 to 5 (Fig. 1), between 10.5° to 8° N and 94° to 88.5° W. Cycles 2 and 4 were near the CRD core, as estimated from satellite imagery of chl *a* and mapping of the flow field with an Acoustic Doppler Current Profiler (ADCP). Cycle 3 was located northeast of the core region, and Cycle 5 was closer to the coast. Despite the geographical differences within the region, environmental variability among the water parcels was not substantial.

Samples for each experiment in each cycle were collected in early morning CTD casts (~02:00 h local time). The undiluted and diluted treatments (d = 1

and d ~ 0.33, respectively, the latter diluted with 0.1 µm Suporcap filtered seawater) were added without nutrient addition to 2.8 l polycarbonate bottles. For each experiment at each depth, only 1 replicate was incubated. Each bottle was incubated for 24 h *in situ*, similar to samples in the CCE, on the satellite-equipped drift array in net bags at the depth and under the natural light and temperature conditions from which the samples were taken. In this study, we focus on samples taken in the mixed later at ~12 m depth. As above, 2 ml samples for FCM analyses were taken from each treatment initially and at the end of the incubation and preserved and frozen for later analysis.

Flow cytometry sample processing

Flow cytometry (FCM) samples from all study regions were processed similarly. FCM samples from each region were thawed, stained with 1 µg ml^{-1} of Hoechst 33342 (Monger & Landry 1993), and analyzed with a Beckman-Coulter EPICS Altra cytometer. Two water-cooled 5 W argon ion lasers were used to deliver simultaneous excitation at 488 nm (1 W) and in the UV range (200 mW). The optical filter configuration provided information on DNA (blue fluorescence, 450 nm), phycoerythrin (orange fluorescence, 575 nm), chl *a* (red fluorescence, 680 nm), and 90°-side and forward light scatter. This information was used to distinguish 3 populations: *Prochlorococcus*, *Synechococcus*, and photosynthetic picoeukaryotes. The light scattering values were normalized with 0.5 µm yellow-green fluorescent beads. To convert normalized light scatter values to cell diameters for the picoplankton assemblage, the median forward light scattering values for *Prochlorococcus* and for *Synechococcus* were regressed against literature-based cell diameters for these taxa: 0.55 µm for *Prochlorococcus* (Partensky et al. 1999) and 0.95 µm for *Synechococcus* (Morel et al. 1993). The resulting relationship was used to assign cell diameter estimates to individual cells. Different regressions using this technique were calculated and used for each study region.

Estimates of size-specific rates and their associated errors

We estimated size-specific phytoplankton growth and microzooplankton grazing rates using a modification of the dilution technique: the size-dependent dilution method (Taniguchi et al. 2012). Specifically, changes in net phytoplankton concentration for different sized organisms are measured according to the equation:

$$\text{net growth rate for size class } i = \frac{1}{t}\ln\left(\frac{P_{t,i}}{P_{0,i}}\right) = \mu_i - dg_i \quad (1)$$

where i = 1, 2, …, n for n size classes, $P_{0,i}$ and $P_{t,i}$ are initial and final phytoplankton concentrations (cells ml^{-1}) for size class i, t is the incubation time (typically 1 d), d is the fraction of unfiltered seawater, and μ_i and g_i are the growth and grazing rates, respectively, for size class i. Phytoplankton were divided into size intervals with bin divisions at 0.45, 0.65, 1.25, 2.75, and 4.00 µm. These size intervals were chosen to correspond approximately to the picoplankton included in this study, specifically *Prochlorococcus*, *Synechococcus*, and small and large picoeukaryotes. Because these FCM data sets are based on 100 µl sample analysis volumes, and therefore only resolve the more numerous pico- and nanoplankton, counts for cells >4 µm are not sufficiently abundant to allow statistically robust rate estimates of larger cells (Taniguchi et al. 2012).

Once the cells were divided into defined size intervals, growth (µ, d^{-1}) and grazing (g, d^{-1}) loss estimates for each size class were computed according to Eq. (1). Following the derivations described by Taniguchi et al. (2012), estimates of the standard deviations for growth (σ_μ), grazing (σ_g) and net growth rate ($\sigma_{\text{net growth}}$) were calculated according to the equations:

$$\sigma_\mu = \frac{1}{t(1-d)}\sqrt{\frac{1}{N_{t,d}} + \frac{1}{N_{0,d}} + d\left(\frac{1}{N_t} + \frac{1}{N_0}\right)} \quad (2)$$

$$\sigma_g = \frac{1}{t(1-d)}\sqrt{\frac{1}{N_{t,d}} + \frac{1}{N_{0,d}} + \frac{1}{N_t} + \frac{1}{N_0}} \quad (3)$$

$$\sigma_{\text{net growth}} = \frac{1}{t}\sqrt{\frac{1}{N_t} + \frac{1}{N_0}} \quad (4)$$

where N_0 is the number of cells in the initial undiluted sample, N_t is the number of cells in the undiluted incubated sample, $N_{0,d}$ is the cell count in the initial diluted treatment, and $N_{t,d}$ is the cell count in the final diluted sample. Applying Eqs. (2), (3) & (4) to each size class provides error estimates for size-specific growth, grazing, and net growth rates, respectively.

Taxon-specific rates

To examine the rates for different taxa, we looked at the groups readily identifiable via flow cytometry,

namely *Prochlorococcus*, *Synechococcus*, and picoeukaryotes. These are also the groups that guided our initial choice of size bins. While the addition of data from other methods, e.g. epifluorescence microscopy or FlowCAM, would increase the number of taxonomic groups and size range under study, we were limited by the samples taken and available data. To mimic allometric studies of monospecific cultures and/or compilations of rate data but still allow comparisons among regions, we combined rate estimates for each taxon in each area. However, because of the strongly differing oceanographic conditions in the CCE, we separated rates from the offshore region (Cycles 2 and 5) and the inshore region (Cycles 1 and 3). Cycle 4, a transitional region, was not included.

Relationship of growth and grazing mortality rates with temperature

To examine the relationship of μ and g with temperature, we used rates averaged across cycles in the CCE and CRD and across the whole EP region. Each taxonomic group, however, was kept separate to compare across taxa. Each averaged rate was then plotted against the associated mean temperature. To see how well MTE can describe the relative change in g with temperature compared to μ, we calculated the theoretical rates. According to MTE, a rate R should scale with temperature according to the equation:

$$R = re^{-E/kT} \quad (5)$$

in which r is the rate coefficient (consisting of R_0 the normalization constant, M the mass, and a the allometric exponent), E the activation energy, k Boltzmann's constant (-8.62×10^5 eV K^{-1}), and T temperature (Brown et al. 2004). We used activation energy estimates of 0.36 eV for μ and 0.67 eV for g (Chen et al. 2012). We used the above equation to solve for the rate coefficient r separately for each taxonomic group. That is, for each taxonomic group, we used the average rate measurements and their corresponding mean temperature values described above in Eq. (5) to calculate their associated r values. Those r values were then averaged to obtain a mean coefficient for each taxonomic group. We then estimated the theoretical rate given its associated temperature, using the appropriate coefficient. While this method of estimating r for each group is somewhat arbitrary, it does provide a consistent method to compare the *relative* amounts of variability explained by temperature for growth versus grazing rates.

RESULTS

Intra-regional size-specific rates

To facilitate the comparison of size-specific μ and g within the CCE and CRD regions, we averaged rates from the separate days of individual experimental cycles. Although this averaging technique makes the rates more conservative by de-emphasizing daily variability, it provides clearer, more robust comparisons among and within geographical regions and is also in keeping with previous treatment of data from separate days of experimental cycles (Landry et al. 2009). Because of the relative constancy of μ, g, and community composition in the EP and the independence of each station estimate (Landry et al. 2011a, Selph et al. 2011), we only considered the regional rate averages for this part of the Pacific. Rules for arithmetic operations on standard deviations were used to determine the errors associated with the mean values. That is, to find the standard deviation of average values, the standard deviations of each individual rate were squared, summed, and the sum square rooted and divided by the number of samples to determine the standard deviation of the mean value.

We could not always fit the data to a typical allometric power law dependence (Gould 1966) because of negative rate values and non-monotonic trends for both growth and grazing rates. Therefore, to highlight rate differences among size classes, we used 2 alternate metrics. First, we fit linear regressions to the size and rate values to determine the sign and significance of the slopes. Second, we compared only the rates and error estimates (±1 SD) for the largest and smallest size classes to determine whether they were different. In the subsequent sections, all rates are given as: rate ±1 SD.

California Current Ecosystem

The CCE showed a wide variation in rates among size classes and cycles for μ, g, and net growth rates (Fig. 2). All μ values together ranged from −0.70 ± 0.17 to 0.83 ± 0.13 d^{-1}, g values from slightly negative to 0.56 ± 0.23 d^{-1}, and net growth rates from −0.67 ± 0.05 to 0.67 ± 0.04 d^{-1}. These rates did not follow consistent trends with size (Fig. 2), though there was significant size variability for some cycles (Table 1). For example, μ decreased with size in Cycles 2 and 5 (both offshore), and increased for Cycle 4 (transitional region; Fig. 2a, Table 1). Cycle 5 was the only one with significant size-dependent variability for g

(decreasing). Net growth rate trends, on the other hand, were all significant except for Cycle 1, and the relationship with size (increasing or decreasing) usually followed the size-dependence of μ (Table 1).

More striking than the size relationships themselves are the similarities and contrasts among cycles in the magnitudes of the rates and the curve shapes, particularly for μ (Fig. 2a). For example, Cycles 1 and 3, both from the inshore region of the CCE, had generally high μ with a slight minimum in the second-smallest size class. Cycle 4, which is considered to be water advected offshore from the direction of Cycle 1, had lower μ values than Cycle 1, and the rates increase monotonically with size (Table 1). The μ values of Cycles 2 and 5, both from the offshore CCE, showed monotonically decreasing patterns (Table 1) with values that were highly negative for the 2 largest size classes.

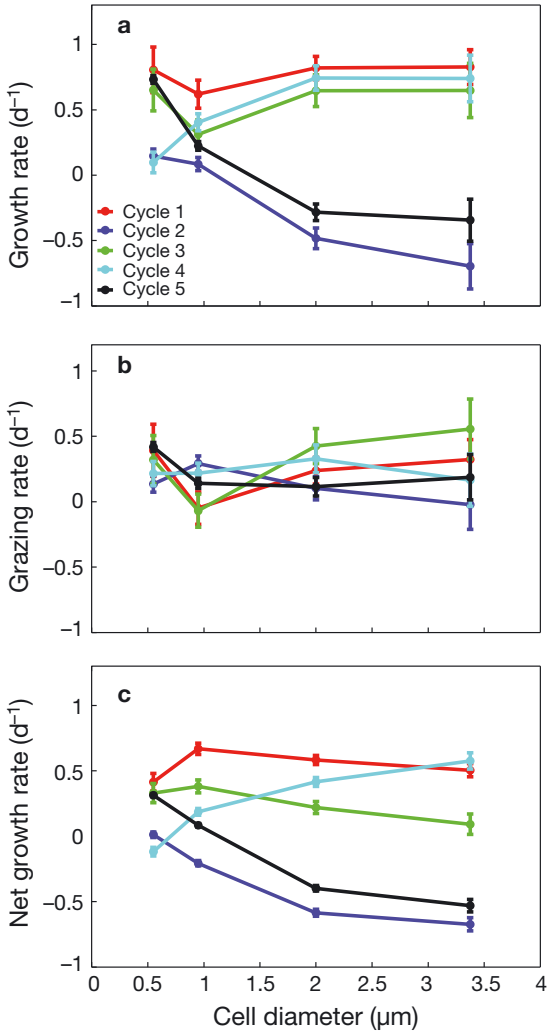

Fig. 2. Size-dependent (a) growth, (b) grazing, and (c) net growth rates in the California Current Ecosystem, averaged for each experimental cycle. Vertical bars are ±1 SD

Table 1. Size-dependent trends in growth, grazing, and net growth rates. The trend is increasing if the rate of the largest size class is significantly greater than that of the smallest size class and decreasing if the opposite is true. CCE: California Current Ecosystem; CRD: Costa Rica Dome; EP: Equatorial Pacific. Dashes represent no significant trend. Asterisk indicates a significant regression between rate and size. In the CCE and CRD, a cycle represents a multi-day experiment in which a water parcel was studied and followed via a satelllite-tracked drift array

Region Cycle	Trend in growth rate	Trend in grazing rate	Trend in net growth rate
Within CCE			
1	–	–	–
2	Decreasing*	–	Decreasing
3	–	–	Decreasing*
4	Increasing	–	Increasing
5	Decreasing	Decreasing	Decreasing
Within CRD			
2	–	–	–
3	Increasing	Increasing	–
4	–	–	–
5	–	–	Decreasing
Average EP	Decreasing	Decreasing	–

For *g* (Fig. 2b), the inshore Cycles 1 and 3 were similar, with depressed values in the second-smallest size class. The other cycles each had different size patterns, but rates generally overlapped within a cycle among at least 3 size classes. Only Cycle 5 (offshore) had a significant decreasing trend with size (Table 1).

Net growth rates (μ – *g*) decreased significantly with size for Cycles 2, 3, and 5 (Fig. 2c, Table 1), while Cycle 4 showed monotonically increasing net growth rates. The patterns of Cycles 2 and 5 were similar to one another, as were those of Cycles 1 and 3.

Costa Rica Dome

Overall, rate estimates for the CRD displayed much less variability with size than in the CCE. μ ranged from 0.45 ± 0.04 to 0.79 ± 0.06 d^{-1}, *g* from 0.53 ± 0.12 to 1.17 ± 0.10 d^{-1}, and net growth rates from –0.46 ± 0.03 to 0.16 ± 0.03 d^{-1} (Fig. 3). The only significant increases of rates with size were for Cycle 3 (both μ and *g*; Fig. 3a,c), and the only significant decrease with size was for net growth in Cycle 5 (Fig. 3e, Table 1).

In terms of the rate magnitudes, Cycles 2 and 3 stand out, but in different ways. Cycle 2, from the core of the CRD, generally had lower μ values, while

Cycle 3, the most offshore sampling region, had higher *g* values. These between-cycle differences for μ and *g* lead to different net growth rates, with Cycle 3 having relatively uniform and strong negative values, Cycles 4 and 5 being slightly net positive, and Cycle 2 in between. Thus the net growth rates of Cycles 2 and 3 were both negative, but for different reasons: Cycle 2 had low μ values relative to the other cycles, while Cycle 3 had the highest *g* values. These differences highlight the importance of measuring the underlying μ and *g* values to interpret net changes in planktonic communities.

Equatorial Pacific

There was little variation in μ and *g* with size in the equatorial Pacific (Fig. 3). μ rates in this region varied from 0.52 ± 0.02 to 0.65 ± 0.02 d^{-1}, *g* rates from 0.62 ± 0.03 to 0.76 ± 0.02 d^{-1}, and net growth rates from −0.11 ± 0.01 to −0.10 ± 0.01 d^{-1}. Both μ and *g* showed general decreases in rates with increasing size (Table 1). Because they showed similar patterns and because *g* was slightly higher than μ for each size class, the net growth rate was negative across the whole size range considered and does not show any size dependence. However, we note that these values are small, in keeping with the near steady state conditions considered typical in this region.

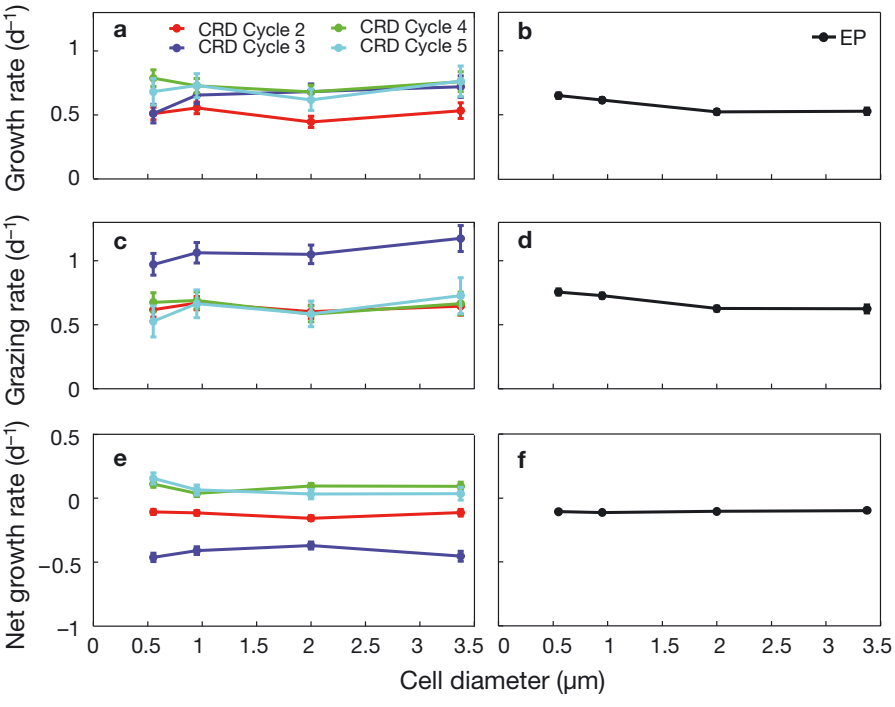

Fig. 3. Size-dependent (a,b) growth, (c,d) grazing, and (e,f) net growth rates in the Costa Rica Dome (left side) and equatorial Pacific (right side). Values from the Costa Rica Dome were averaged for each experimental cycle, and those in the equatorial Pacific were averaged over the whole region. Bars are ±1 SD; some bars are not visible. Note different *y*-axis scale in panels e,f

Inter-regional size-specific rates

Among μ rates, the CRD (Fig. 3a) and the EP (Fig. 3b) showed similarly low variation among sizes. μ rates in the CCE showed more marked changes with size among all cycles (Fig. 2a). The CRD, EP, and Cycles 1 and 3 (the inshore stations) of the CCE almost all had high μ values, between ~0.5 and 0.8 d^{-1}, with the exception of the second-smallest size class of Cycle 3 in the CCE and the second-largest size class of Cycle 2 in the CRD. By comparison, μ values for the offshore CCE (Cycles 2 and 5) decreased more markedly with increasing size (Table 1) and were the only areas that had negative μ values.

Among *g* rates, CCE values (Fig. 2b) again showed more variability among size classes than rates in either the CRD (Fig. 3c) or EP (Fig. 3d). Still, this variability was less than that seen in the CCE μ rates. The tropical regions, the EP and CRD, generally had higher *g* values (>0.5 d^{-1}) than in the CCE (< ca. 0.4 d^{-1}, except for the largest size class of Cycle 3). Cycle 5 of the CCE and the EP both showed decreases in *g* with increasing size (Table 1), but the decrease was greater in the CCE region.

Net growth rates in the EP (Fig. 3f) and CRD (Fig. 3e) were all negative or on the order of 0.1 d^{-1} and were all relatively uniform across size classes. The CCE net growth rates (Fig. 2c), however, often varied more widely compared to the other regions, from as much as −0.53 to 0.31 in Cycle 5 (an offshore station) and −0.12 to 0.58 d^{-1} in Cycle 4 (the transitional station). Only the inshore stations (Cycles 1 and 3) had positive net growth rates for all size classes.

Taxon-specific rates

Prochlorococcus μ values (mean ± SD) ranged between 0.17 ± 0.12 d^{-1} in the inshore area of the CCE to 0.59 ± 0.01 d^{-1} in the EP (Fig. 4a). *Synechococcus* μ values ranged from 0.68 ± 0.03 d^{-1} in the CRD to 0.97 ± 0.04 d^{-1}

in the EP. *Prochlorococcus* consistently had a lower mean μ rate than *Synechococcus* in all regions. Except in the EP, μ values of *Prochlorococcus* were the lowest of all cell types. However, we note that there was also large variability in *Prochlorococcus* μ values, particularly in the inshore and offshore CCE. Picoeukaryote μ rates ranged from 0.46 ± 0.13 d^{-1} in the offshore CCE to 1.03 ± 0.06 d^{-1} in the CRD. Although picoeukaryotes had higher μ rates than *Prochlorococcus,* there was no consistent pattern when comparing *Synechococcus* and picoeukaryotes. Aggregate μ values for all cells combined ranged from 0.45 ± 0.03 d^{-1} in the offshore CCE to 0.65 ± 0.02 d^{-1} in the CRD.

For *g* (Fig. 4b), *Prochlorococcus* values ranged from 0.02 ± 0.12 d^{-1} in the offshore CCE to 0.66 ± 0.02 d^{-1} in the EP. *Synechococcus g* rates ranged from 0.24 ± 0.08 d^{-1} in the inshore CCE to ~0.92 d^{-1} in all other regions. Picoeukaryote *g* values were lowest in the inshore CCE at 0.19 ± 0.10 d^{-1} and were 0.78 ± 0.09 d^{-1} in the EP. For all cells combined, again, the *g* rates in the inshore CCE were lowest (0.16 ± 0.05 d^{-1}), and CRD rates highest (0.75 ± 0.02 d^{-1}). In most regions, *Synechococcus* experienced the highest *g* rates, with the exception of the inshore CCE.

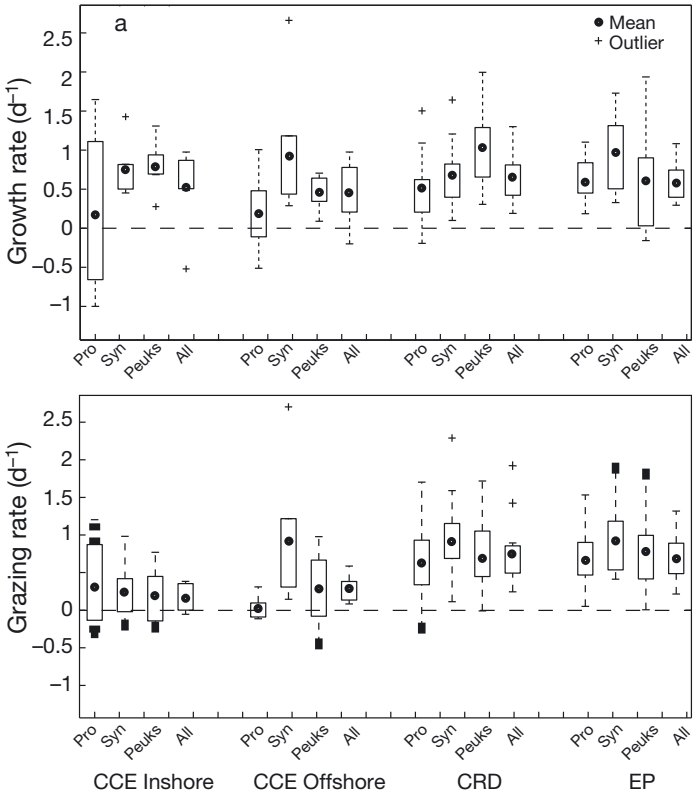

Fig. 4. (a) Growth and (b) grazing rates among taxa for each study region, averaged over all experiments in each region. The boxes indicate the 25 and 75% percentiles, and the dotted vertical lines represent that minimum and maximum rate values not considered outliers. The zero line is indicated by the horizontal dashed line. In each region, taxonomic groups are ordered as *Prochlorococcus* (Pro), *Synechococcus* (Syn), picoeukaryotes (Peuks), and all taxonomic groups combined (All). CCE: California Current Ecosystem; CRD: Costa Rica Dome; EP: equatorial Pacific

Relationship of growth and grazing mortality rates with temperature

In general, both μ and *g* for most cell types appeared to increase with increasing temperature (Fig. 5), although there is noticeable variability, particularly at lower temperatures. When comparing the theoretical relationship of temperature versus μ (Fig. 5a), growth variability was only partially explained by temperature, with r^2 values ranging from ~0.2 for *Prochlorococcus* and picoeukaryotes to –0.76 for *Synechococcus*. This particularly low value was largely driven by high growth at 14.4°C. If that rate was removed, the coefficient of determination was –0.01.

For *g*, more of the variability was explained by temperature (Fig. 5b). As much as 82% of the variation in *g* for all cell types combined was described by the theoretical temperature relationship. Again, *Synechococcus* had the lowest coefficient of determination, but if the value at 14.4°C was omitted, r^2 increased to 0.62.

DISCUSSION

Size-specific trends in growth and grazing rates

Classic allometric studies using compilations of laboratory measurements predict that growth (μ) and grazing (*g*) rates decrease monotonically over several orders of magnitude in size (Fenchel 1974, Tang 1995, Hansen et al. 1997). More recent evidence suggests such traditional patterns may not hold among the picoplankton, and instead μ and *g* may correlate positively (Raven 1994, Bec et al. 2008, Chen & Liu 2010) or isometrically (Huete-Ortega et al. 2012) with size. In this study, we found no consistent scaling of either μ or *g* with cell diameter (Figs. 2 & 3).

There are several non-mutually exclusive reasons for this lack of size dependence. Even for rates, particularly μ, measured over relatively wide size ranges in controlled laboratory settings, the exact relationships and strength of size trends are controversial (Banse 1982, Sommer 1989, Chisholm 1992, although

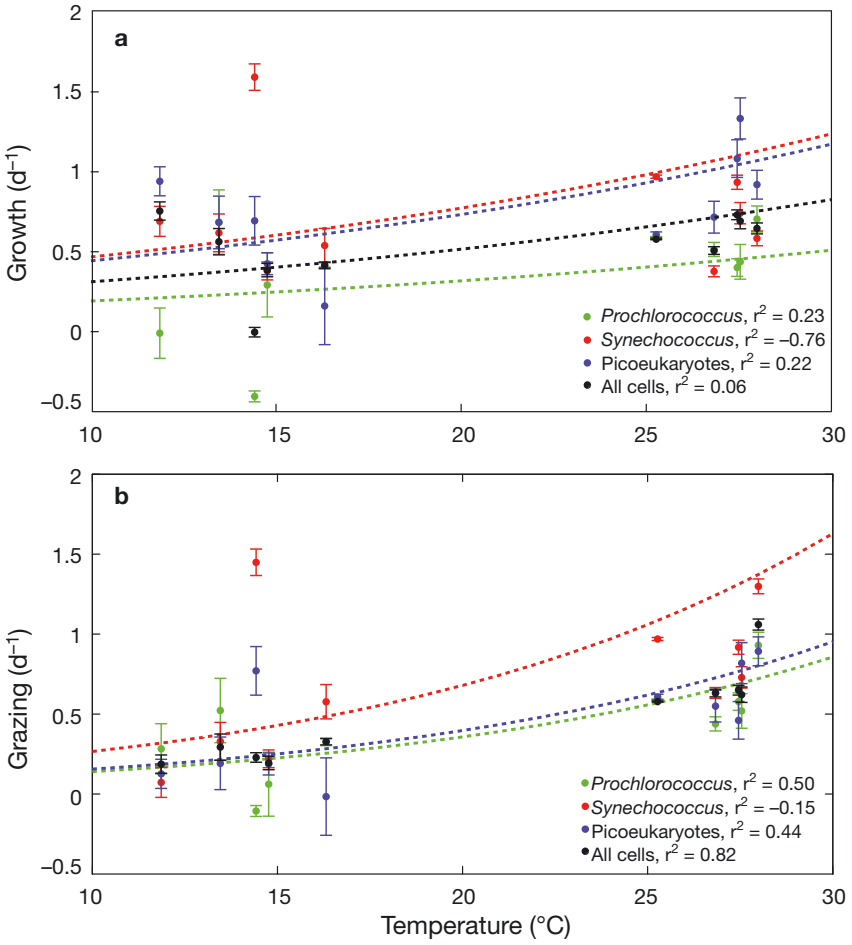

Fig. 5. The relationship of taxon-specific (a) growth and (b) grazing rates with temperature. For each cell type, the correspondingly colored dotted lines show the theoretical relationships of each rate with temperature according to the relationship $R = re^{-E/kT}$ (R: metabolic rate, r: rate coefficient, E: activation energy, k: Bolzmann's constant, and T: temperature)

see Mizuno 1991). Our lack of size dependency may, therefore, be because our size range (0.45 to 4.0 µm) is too narrow (Tilman et al. 2004) and/or because our rates are measured in the field, where other factors override the effects of size variability. Our realized µ and *g* potentially reflect suboptimal conditions and hence may inherently display different patterns than maximal rates. Furthermore, in natural assemblages, systematic changes in rates with size may also be masked by changes in community structure. For example, while µ rates of eukaryotes tend to decrease with size, there is evidence that the opposite is true for prokaryotic cells (DeLong et al. 2010, Kempes et al. 2012, although see Nielsen 2006). Because our size-dependent rates pooled prokaryotes and eukaryotes together, variable fractions of the different cell types among size classes could have led to differences in trends with size. However, we did not observe consistent trends when examining taxon-specific rates (Fig. 4).

Chen & Liu (2010), however, found systematic trends in µ and *g* from a global synthesis of rates measured from the dilution method as well as ^{14}C uptake. Without considering any taxonomic divisions, µ values of natural phytoplankton communities followed a unimodal pattern, with cells of 2.8 µm (based on dilution method data) or 5.4 µm (based on ^{14}C uptake experiments) diameter having the highest µ values. Our cell size range overlaps the inflection point in the dilution relationship, and our different approach for assigning growth rates to organism size could obscure a consistent size trend. Nonetheless, it is fair to say that the lack of a systematic effect of size on µ for natural assemblages that include *Prochlorococcus*, *Synechococcus*, and small photosynthetic eukaryotes is unexpected (Raven et al. 2005, Zubkov et al. 2007).

Chen & Liu (2010) further observed that *g* increased with increasing size, in contrast to the prevailing view of reduced grazing efficiency by microherbivores on larger phytoplankton cells. Among cells of picoplankton size, such a trend (reduced grazing mortality impact on smaller cells) would be consistent with small size providing a grazing refuge due to reduced random encounters with flagellate cells that feed by direct interception (e.g. Banse 1982, Monger & Landry 1990). Again, the lack of a clear systematic trend in grazing vulnerability with size would seem to suggest that either the size range of cells examined was too small to assess size-dependent trends with sufficient precision to see patterns, or that the diversity of consumers, the varying efficacies of grazer-deterrent strategies of prey, or other environmental complexities were sufficiently powerful to override the pure effects of size.

To examine if there were any trends in taxon-specific rates, we also estimated µ and *g* rates for *Prochlorococcus*, *Synechococcus*, picoeukaryotes, and, for completeness, all cell types combined (Fig. 4).

For each region examined, *Prochlorococcus*—the smallest cell type—had lower μ rates than *Synechococcus* and picoeukaryotes. However *Prochlorococcus* rates were notably variable in the CCE. In addition, relationships were inconsistent for the other 2 groups.

Rates in different regions of the Pacific

Among experimental regions in the present study, variability in average μ values was highest in the CCE (Fig. 2a). The high μ values for Cycles 1, 3, and 4, compared to Cycles 2 and 5, and the larger overlap in average *g* values among cycles align with bulk community rates based on chl *a* measurements (Landry et al. 2009). Similarly, picoeukaryotes and all cells combined from the inshore CCE had higher μ rates than offshore (Fig. 4a).

In the CCE, the negative μ rates for cells >1.25 μm (Fig. 2a) may indicate sub-optimal growth conditions, bottle effects, or losses that are unaccounted for by the dilution method, such as programmed cell death or viral lysis (Weinbauer & Hofle 1998, Bidle & Falkowski 2004).

We also argue that strongly decreasing patterns seen for the size-dependent μ rates in the offshore CCE may be influenced by nutrient availability. In this region, nitrate is the main limiting nutrient (Eppley et al. 1979). Cycles 2 and 5 in the offshore area of the CCE had deep nitraclines compared to the other sampling regions (Landry et al. 2009). If nitracline depth can be used as a proxy for nutrient availability, the deep nitracline (i.e. low nutrient conditions) found offshore are expected to be disadvantageous for larger cells compared to smaller cells, based on relative surface area to volume ratios for nutrient uptake. Thus, the strongly decreasing μ rates with increasing size in the offshore CCE region is consistent with the expected response to nutrient limitation. That these patterns are not clear for taxon-specific rates suggests significant overlap of taxa among size classes.

Two other studies have also examined picophytoplankton μ and *g* rates in the CCE. Worden & Binder (2003) measured μ and *g* for *Prochlorococcus* and *Synechococcus* in the open ocean in September 1998. Their rate values were substantially higher than the size-dependent offshore rates measured in our springtime study. However, our taxon-specific μ and *g* rates for *Synechococcus* and *Prochlorococcus* were more extreme than previous measurements. In Worden et al. (2004), both growth and grazing rates of cyanobacteria and picoeukaryotes measured in nearshore waters from the Scripps pier (La Jolla, California) showed high variability over a 2 yr study period. The inshore CCE μ and *g* rates for all the cell types measured in this study fell within the range of rates measured in Worden et al. (2004). The offshore taxon-specific rates fell outside the range previously measured. Taken together, the wide range in μ and *g* among the studies mentioned above as well as this present study reflect high spatial and temporal variability in the dynamic CCE.

Despite this variability, the inshore experimental cycles (Cycles 1 and 3) showed size-dependent trends more similar to one another compared to the offshore regions, particularly with respect to μ (Fig. 2a). The offshore sampling areas, Cycles 2 and 5, also showed similar size-specific patterns to one another, while the transitional water parcel, Cycle 4, was distinct. Therefore, despite pronounced variability for the region as a whole, independent experiments in water parcels experiencing roughly similar environmental conditions gave relatively similar patterns in size-specific rates, suggesting that the relative rate behaviors of size classes are linked to differences in growth conditions or community compositions within the subregions.

Within the CRD, similarity within subregions is also apparent (Fig. 3). For example, Cycles 3, 4, and 5 had similar size-dependent growth rate patterns, while Cycles 2, 4, and 5 had similar *g* rates. The lack of more distinct water-parcel differences in the CRD likely reflects the more subtle range of environmental variability compared to the CCE.

Community μ rates based on chl *a* for the equatorial Pacific, which ranged from 0.71 to 0.84 d^{-1} (Selph et al. 2011), were slightly higher than the size-specific and most taxon-specific cell-based measurements of this study. This reflects the higher μ values of eukaryotes, particularly diatoms, that were included in the community μ (Landry et al. 2011a), but excluded from the community growth rates of the present study. Conversely, the lower bound for size- and taxon-specific *g* values in this study is comparable to the mean community *g* estimate of ~0.60 d^{-1} (Selph et al. 2011), with the difference explained by lower microzooplankton grazing impacts on the larger eukaryotes (Landry et al. 2011a). Although this region showed slight decreases in μ and *g* with increasing size (Table 1, Taniguchi et al. 2012), the overall range in rates was relatively small compared to the CCE.

Because rate information from previous studies in the CRD is lacking, we had little basis upon which to

draw a strong experimentally based distinction between the CRD and EP regions. Both are tropical, open-ocean upwelling systems, exhibiting dominance by picoplankton and micronutrient limitation. Therefore, despite some compositional differences, notably the very high concentrations of *Synechococcus* in the CRD (Li et al. 1983, Saito et al. 2005), the close correspondence between measured rates in these 2 regions (Fig. 3) suggests that they function similarly with respect to size-based patterns of picophytoplankton dynamics. Both regions also have similar taxon-based rates, particularly *g* rates (Fig. 4b). Both regions had similarly depressed *Prochlorococcus* μ rates; in the CRD the picoeukaryotes had the highest μ rates while in the EP *Synechococcus* had the highest μ rate. Nevertheless, their community μ and *g* were similar.

Size-specific μ rates, and to a certain extent *g* rates, among cycles in the CCE were more variable than rates both among cycles in the CRD and also between the CRD and EP. Because these rates are realized rates measured in the field, the difference in variability likely reflects, and thus highlights, the differing environmental conditions that exist across these regions of the eastern Pacific. The variable rates in the CCE are likely due to the dynamic environmental conditions seen in the region, and contrastingly, to the much less variable conditions measured within the CRD and in the EP. Another characteristic of the EP and CRD experiments was the near zero net growth rate of the regional averages (Fig. 3e,f), which is indicative of the tight coupling between picophytoplankton and their microzooplankton grazers in these systems (Landry et al. 1995a, Landry et al. 1997, Landry 2002, Landry et al. 2011a, Selph et al. 2011).

Temperature relationships of growth and grazing rates

While we cannot prove that the type of rate data that we generated should necessarily follow the theoretical functional relationships of the MTE (as discussed further below), we did find that MTE-based temperature corrections for our experiments done in different systems were able to explain much more of the variability in μ and *g* for all cell types (Fig. 5). This result is consistent with expectations that the temperature sensitivities of heterotrophic and autotrophic processes may differ because they are regulated by different rate-limiting biochemical reactions (Allen et al. 2005, López-Urrutia et al. 2006). According to the MTE (Brown et al. 2004), the activation energy (~0.6 to 0.7 eV) for heterotrophic processes is usually limited by the production of ATP from glycolysis and the tricarboxylic acid (TCA) cycle. For photoautotrophs, however, temperature-driven antagonistic effects of oxygen and carbon dioxide binding with ribulose bisphosphate carboxylase oxygenase (Rubisco) during photosynthesis lead to a lower activation energy of ~0.32 eV (Allen et al. 2005, López-Urrutia et al. 2006). Based on theory, therefore, temperature–rate relationships for heterotrophic processes may be steeper and more likely significant when compared to those for autotrophs.

Though our results are in accordance with this hypothesis (Fig. 5), there is ongoing debate about the validity or applicability of the MTE. In marine systems, for example, Rose & Caron (2007) demonstrated that heterotrophic protists were more acutely affected by temperature than autotrophs, and López-Urrutia (2008) showed how the activation energies derived from the same data were similar to those predicted by the MTE. However, Caron & Rose (2008) subsequently argued that the mechanistic constraints on process rates in complex natural plankton communities are broader than temperature and that the equilibrium conditions assumed by the MTE may not apply to transient, bloom-dominated datasets (see also Cottingham & Zens 2004). Additional broader concerns about the MTE include whether its relationships hold over smaller ranges (Tilman et al. 2004), and whether the model is mechanistic, phenomenological, or somewhere in between (Cyr & Walker 2004, O'Connor et al. 2007).

Despite these criticisms, the MTE does provide a framework for a relative comparison of μ and *g* versus temperature. Should this comparison hold, the implication of a higher temperature influence on grazing over growth may become increasingly important under future climatic conditions. Warming and stratification are suggested to alter population structures in different regions of the world's oceans. According to Marañón et al. (2012), small phytoplankton are expected to increase in non-light limited areas that experience greater stratification and subsequently more limited nutrient input. However, if grazing mortality rates also increase, particularly at a faster rate than growth rates, this increase in small phytoplankton may be mitigated. While the present study does not examine grazing on larger phytoplankton, if this same relationship extends to larger grazers (Sommer & Lengfellner 2008), the increased populations of larger phytoplankton expected in light-limited regions and coastal eutrophication sites

may also be less extensive than anticipated under future climate change. However, because temperature might also increase the rates at which consumers prey on one another, the overall effect of temperature on planktonic biomass and community size structure is not easily predictable.

CONCLUSIONS

In summary, μ and *g* for picophytoplankton in the CCE showed high variability, while CRD and EP rate estimates were less variable, with net growth rates typically near zero. Mean μ rates of *Prochlorococcus* were always lower than those of *Synechococcus*, but other taxon-specific comparisons of μ and *g* were inconsistent across regions. Temperature explained more of the variation in *g* than in μ. Within the cell size range examined, size-dependent trends were not a general feature of μ or *g* in any of the 3 study regions, but strong size-dependent trends were found in experiments conducted within the offshore CCE water, consistent with possible nutrient limitation of larger picophytoplankton cells in this area.

Although size-dependent rates were not typical within the natural picophytoplankton assemblages of the systems studied, size is nonetheless important for assessing the affects of environmental variability on planktonic rates. Given projected changes in the size structure of planktonic communities (Marañón et al. 2012) and the importance of size in many fundamental processes (e.g. feeding, carbon export), it is imperative to understand how size variability in natural ecosystems is shaped by environmental conditions and community dynamics and influences biogeochemical fluxes. To fully understand the ecosystem characteristics that most influence planktonic populations and to ultimately model their dynamics under variable climatic conditions, future studies should examine in more detail the interactive effects of size, species composition, environmental variability, and process rates.

Acknowledgements. We thank the Captain and crew of the R/V 'Melville' and R/V 'Revelle' for their generous assistance and support at sea. We also thank Mark Ohman for his helpful comments on the manuscript, as well as colleagues who contributed to shipboard experiments in the Equatorial Biocomplexity, CCE-LTER, and Costa Rica Dome FLUZiE (Flux and Zinc Experiments) programs. We also thank Emilio Marañón and 2 other anonymous reviewers for their helpful critiques. This work was supported by these 3 projects with funding from U.S. National Science Foundation grants OCE 0322074, 0417616, and 0826626, respectively.

LITERATURE CITED

Allen AP, Gillooly JF, Brown JH (2005) Linking the global carbon cycle to individual metabolism. Funct Ecol 19: 202–213

Banse K (1976) Rates of growth, respiration and photosynthesis of unicellular algae as related to cell-size—a review. J Phycol 12:135–140

Banse K (1982) Cell volumes, maximal growth rates of unicellular algae and ciliates, and the role of ciliates in the marine pelagial. Limnol Oceanogr 27:1059–1071

Barber RT, Sanderson MP, Lindley ST, Chai F and others (1996) Primary productivity and its regulation in the equatorial Pacific during and following the 1991–1992 El Nino. Deep-Sea Res II 43:933–969

Bec B, Collos Y, Vaquer A, Mouillot D, Souchu P (2008) Growth rate peaks at intermediate cell size in marine photosynthetic picoeukaryotes. Limnol Oceanogr 53: 863–867

Bidle KD, Falkowski PG (2004) Cell death in planktonic, photosynthetic microorganisms. Nat Rev Microbiol 2:643–655

Brown JH, Gillooly JF, Allen AP, Savage VM, West GB (2004) Toward a metabolic theory of ecology. Ecology 85: 1771–1789

Caron DA, Rose JM (2008) The metabolic theory of ecology and algal bloom formation (Reply to comment by López-Urrutia). Limnol Oceanogr 53:2048–2049

Caron DA, Dennett MR, Lonsdale DJ, Moran DM, Shalapyonok L (2000) Microzooplankton herbivory in the Ross Sea, Antarctica. Deep-Sea Res II 47:3249–3272

Cavender-Bares KK, Rinaldo A, Chisholm SW (2001) Microbial size spectra from natural and nutrient enriched ecosystems. Limnol Oceanogr 46:778–789

Chen B, Liu H (2010) Relationships between phytoplankton growth and cell size in surface oceans: interactive effects of temperature, nutrients, and grazing. Limnol Oceanogr 55:965–972

Chen B, Landry MR, Huang B, Liu H (2012) Does warming enhance the effect of microzooplankton grazing on marine phytoplankton in the ocean? Limnol Oceanogr 57: 519–526

Chisholm SW (1992) Phytoplankton size. In: Falkowski PG, Woodhead AD (eds) Environmental science research; primary productivity and biogeochemical cycles in the sea. Plenum Press, New York, NY

Coale KH, Fitzwater SE, Gordon RM, Johnson KS, Barber RT (1996) Control of community growth and export production by upwelled iron in the equatorial Pacific Ocean. Nature 379:621–624

Cottingham KL, Zens MS (2004) Metabolic rate opens a grand vista on ecology. Ecology 85:1805–1807

Cyr H, Walker SC (2004) An illusion of mechanistic understanding. Ecology 85:1802–1804

DeLong JP, Okie JG, Moses ME, Sibly RM, Brown JH (2010) Shifts in metabolic scaling, production, and efficiency across major evolutionary transitions of life. Proc Natl Acad Sci USA 107:12941–12945

Edwards KF, Thomas MK, Klausmeier CA, Litchman E (2012) Allometric scaling and taxonomic variation in nutrient utilization traits and maximum growth rate of phytoplankton. Limnol Oceanogr 57:554–566

Elser JJ, Marzolf ER, Goldman CR (1990) Phosphorus and nitrogen limitation of phytoplankton growth in fresh waters of North America: a review and critque of experimental enrichments. Can J Fish Aquat Sci 47:1468–1477

Eppley RW (1972) Temperature and phytoplankton growth in the sea. Fish Bull 70:1063–1085

Eppley RW, Sloan PR (1966) Growth rates of marine phytoplankton: correlation with light absorption by cell chlorophyll *a*. Physiol Plant 19:47–59

Eppley RW, Renger EH, Harrison WG (1979) Nitrate and phytoplankton production in southern California coastal waters. Limnol Oceanogr 24:483–494

Fenchel T (1974) Intrinsic rate of natural increase: relationship with body size. Oecologia 14:317–326

Fiedler PC (2002) The annual cycle and biological effects of the Costa Rica Dome. Deep-Sea Res I 49:321–338

Gould SJ (1966) Allometry and size in ontogeny and phylogeny. Biol Rev Camb Philos Soc 41:587–640

Hansen PJ, Bjornsen PK, Hansen BW (1997) Zooplankton grazing and growth: scaling within the 2–2000 µm body size range. Limnol Oceanogr 42:687–704

Hickey BM (1979) The California Current System—hypotheses and facts. Prog Oceanogr 8:191–279

Hofmann EE, Busalacchi AJ, Obrien JJ (1981) Wind generation of the Costa Rica Dome. Science 214:552–554

Huete-Ortega M, Maranon E, Varela M, Bode A (2010) General patterns in the size scaling of phytoplankton abundance in coastal waters during a 10-year time series. J Plankton Res 32:1–14

Huete-Ortega M, Cermeno P, Calvo-Diaz A, Maranon E (2012) Isometric size-scaling of metabolic rate and the size abundance distribution of phytoplankton. Proc R Soc Ser B 279:1815–1823

Jassby AD, Platt T (1976) Mathematical formulation of the relationship between photosynthesis and light for phytoplankton. Limnol Oceanogr 21:540–547

Kempes CP, Dutkiewicz S, Follows MJ (2012) Growth, metabolic partitioning, and the size of microorganisms. Proc Natl Acad Sci USA 109:495–500

Landry MR (2002) Integrating classical and microbial food web concepts: evolving views from the open-ocean tropical Pacific. Hydrobiologia 480:29–39

Landry MR, Hassett RP (1982) Estimating the grazing impact of marine micro-zooplankton. Mar Biol 67:283–288

Landry MR, Constantinou J, Kirshtein J (1995a) Microzooplankton grazing in the central equatorial Pacific during February and August, 1992. Deep-Sea Res II 42:657–671

Landry MR, Kirshtein J, Constantinou J (1995b) A refined dilution technique for measuring the community grazing impact of microzooplankton, with experimental tests in the central equatorial Pacific. Mar Ecol Prog Ser 120:53–63

Landry MR, Barber RT, Bidigare RR, Chai F and others (1997) Iron and grazing constraints on primary production in the central equatorial Pacific: an EqPac synthesis. Limnol Oceanogr 42:405–418

Landry MR, Constantinou J, Latasa M, Brown SL, Bidigare RR, Ondrusek ME (2000) Biological response to iron fertilization in the eastern equatorial Pacific (IronEx II). III. Dynamics of phytoplankton growth and microzooplankton grazing. Mar Ecol Prog Ser 201:57–72

Landry MR, Brown SL, Rii YM, Selph KE, Bidigare RR, Yang EJ, Simmons MP (2008) Depth-stratified phytoplankton dynamics in Cyclone Opal, a subtropical mesoscale eddy. Deep-Sea Res II 55:1348–1359

Landry MR, Ohman MD, Goericke R, Stukel MR, Tsyrklevich K (2009) Lagrangian studies of phytoplankton growth and grazing relationships in a coastal upwelling ecosystem off Southern California. Prog Oceanogr 83: 208–216

Landry MR, Selph KE, Taylor AG, Decima M, Balch WM, Bidigare RR (2011a) Phytoplankton growth, grazing and production balances in the HNLC equatorial Pacific. Deep-Sea Res II 58:524–535

Landry MR, Selph KE, Yang EJ (2011b) Decoupled phytoplankton growth and microzooplankton grazing in the deep euphotic zone of the eastern equatorial Pacific. Mar Ecol Prog Ser 421:13–24

Lawrence C, Menden-Deuer S (2012) Drivers of protistan grazing pressure: seasonal signals of plankton community composition and environmental conditions. Mar Ecol Prog Ser 459:39–52

Li WKW, Rao DVS, Harrison WG, Smith JC, Cullen JJ, Irwin B, Platt T (1983) Autotrophic picoplankton in the tropical ocean. Science 219:292–295

Litchman E, Klausmeier CA, Bossard P (2004) Phytoplankton nutrient competition under dynamic light regimes. Limnol Oceanogr 49:1457–1462

López-Urrutia A (2008) The metabolic theory of ecology and algal bloom formation. Limnol Oceanogr 53:2046–2047

López-Urrutia A, San Martin E, Harris RP, Irigoien X (2006) Scaling the metabolic balance of the oceans. Proc Natl Acad Sci USA 103:8739–8744

Lynn RJ, Simpson JJ (1987) The California Current System: the seasonal variability of its physical characteristics. J Geophys Res 92:12947–12966

Marañón E, Cermeno P, Rodriguez J, Zubkov MV, Harris RP (2007) Scaling of phytoplankton photosynthesis and cell size in the ocean. Limnol Oceanogr 52: 2190–2198

Marañón E, Cermeno P, Latasa M, Tadonleke RD (2012) Temperature, resources, and phytoplankton size structure in the ocean. Limnol Oceanogr 57:1266–1278

Marañón E, Cermeno P, Lopez-Sandoval DC, Rodriguez-Ramos T and others (2013) Unimodal size scaling of phytoplankton growth and the size dependence of nutrient uptake and use. Ecol Lett 16:371–379

Martin JH, Fitzwater SE (1988) Iron deficiency limits phytoplankton growth in the north-east Pacific subarctic. Nature 331:341–343

Mizuno M (1991) Influence of cell volume on the growth and size reduction of marine and estuarine diatoms. J Phycol 27:473–478

Monger BC, Landry MR (1990) Direct-interception feeding by marine zooflagellates: the importance of surface and hydrodynamic-forces. Mar Ecol Prog Ser 65:123–140

Monger BC, Landry MR (1993) Flow cytometric analysis of marine bacteria with Hoechst 33342. Appl Environ Microbiol 59:905–911

Morel A, Ahn YH, Partensky F, Vaulot D, Claustre H (1993) *Prochlorococcus* and *Synechococcus*: a comparative study of their optical properties in relation to their size and pigmentation. J Mar Res 51:617–649

Nelson DM, Landry MR (2011) Regulation of phytoplankton production and upper-ocean biogeochemistry in the eastern equatorial Pacific: introduction to results of the Equatorial Biocomplexity project. Deep-Sea Res II 58: 277–283

Nielsen SL (2006) Size-dependent growth rates in eukaryotic and prokaryotic algae exemplified by green algae and cyanobacteria: comparisons between unicells and colonial growth forms. J Plankton Res 28:489–498

O'Connor MP, Kemp SJ, Agosta SJ, Hansen F and others (2007) Reconsidering the mechanistic basis of the metabolic theory of ecology. Oikos 116:1058–1072

Partensky F, Hess WR, Vaulot D (1999) Prochlorococcus, a marine photosynthetic prokaryote of global significance. Microbiol Mol Biol Rev 63:106–127

Pecseli HL, Trulsen J, Fiksen O (2012) Predator-prey encounter and capture rates for plankton in turbulent environments. Prog Oceanogr 101:14–32

Pomeroy LR, Williams PJI, Azam F, Hobbie JE (2007) The microbial loop. Oceanography 20:28–33

Raven JA (1994) Why are there no picoplanktonic O_2 evolvers with volumes less than 10^{-19} m^3? J Plankton Res 16:565–580

Raven JA (1998) The twelfth Tansley Lecture. Small is beautiful: the picophytoplankton. Funct Ecol 12:503–513

Raven JA, Finkel ZV, Irwin AJ (2005) Picophytoplankton: bottom-up and top-down controls on ecology and evolution. Vie Milieu 55:209–215

Rhee GY, Gotham IJ (1981) The effect of environmental factors on phytoplantkon growth: temperature and the interactions of temperature with nutrient limitation. Limnol Oceanogr 26:635–648

Riegman R, Stolte W, Noordeloos AAM, Slezak D (2000) Nutrient uptake, and alkaline phosphate (EC 3: 1: 3: 1) activity of *Emiliania huxleyi* (Prymnesiophyceae) during growth under N and P limitation in continuous cultures. J Phycol 36:87–96

Rodriguez J, Mullin MM (1986) Relation between biomass and body weight of plankton in a steady-state oceanic ecosystem. Limnol Oceanogr 31:361–370

Rose JM, Caron DA (2007) Does low temperature constrain the growth rates of heterotrophic protists? Evidence and implications for algal blooms in cold waters. Limnol Oceanogr 52:886–895

Rose JM, Feng Y, Gobler CJ, Gutierrez R, Hare CE, Leblanc K, Hutchins DA (2009) Effects of increased pCO_2 and temperature on the North Atlantic spring bloom. II. Microzooplankton abundance and grazing. Mar Ecol Prog Ser 388:27–40

Rothschild BJ, Osborn TR (1988) Small-scale turbulence and plankton contact rates. J Plankton Res 10:465–474

Rykaczewski RR, Checkley DM (2008) Influence of ocean winds on the pelagic ecosystem in upwelling regions. Proc Natl Acad Sci USA 105:1965–1970

Saito MA, Rocap G, Moffett JW (2005) Production of cobalt binding ligands in a *Synechococcus* feature at the Costa Rica upwelling dome. Limnol Oceanogr 50:279–290

Saito H, Ota T, Suzuki K, Nishioka J, Tsuda A (2006) Role of heterotrophic dinoflagellate *Gyrodinium* sp in the fate of an iron induced diatom bloom. Geophys Res Lett 33: L09602, doi: 10.1029/2005SGLO25366

Selph KE, Landry MR, Taylor AG, Yang EJ and others (2011) Spatially-resolved taxon-specific phytoplankton production and grazing dynamics in relation to iron distributions in the Equatorial Pacific between 110 and 140° W. Deep-Sea Res II 58:358–377

Sherr EB, Sherr BF (2007) Heterotrophic dinoflagellates: a significant component of microzooplankton biomass and major grazers of diatoms in the sea. Mar Ecol Prog Ser 352:187–197

Sommer U (1989) Maximal growth rates of Antarctic phytoplankton: only weak depenence on cell size. Limnol Oceanogr 34:1109–1112

Sommer U, Lengfellner K (2008) Climate change and the timing, magnitude, and composition of the phytoplankton spring bloom. Glob Change Biol 14:1199–1208

Sunda WG, Huntsman SA (1997) Interrelated influence of iron, light and cell size on marine phytoplankton growth. Nature 390:389–392

Tang EPY (1995) The allometry of algal growth rates. J Plankton Res 17:1325–1335

Taniguchi DAA, Franks PJS, Landry MR (2012) Estimating size-dependent growth and grazing rates and their associated errors using the dilution method. Limnol Oceanogr Methods 10:868–881

Tilman D, Hillerislambers J, Harpole S, Dybzinski R, Fargione J, Clark C, Lehman C (2004) Does metabolic theory apply to community ecology? It's a matter of scale. Ecology 85:1797–1799

Umatani S, Yamagata T (1991) Response of the Eastern Tropical Pacific to meridional migration of the ITCZ: the generation of the Costa Rica Dome. J Phys Oceanogr 21: 346–363

Vidal J (1980) Physioecology of zooplankton 1. Effects of phytoplankton concentration, temperature, and body size on the growth rate of *Calanus pacificus* and *Pseudocalanus* spp. Mar Biol 56:111–134

Weinbauer MG, Hofle MG (1998) Size-specific mortality of lake bacterioplankton by natural virus communities. Aquat Microb Ecol 15:103–113

Worden AZ, Binder BJ (2003) Application of dilution experiments for measuring growth and mortality rates among *Prochlorococcus* and *Synechococcus* populations in oligotrophic environments. Aquat Microb Ecol 30:159–174

Worden AZ, Nolan JK, Palenik B (2004) Assessing the dynamics and ecology of marine picophytoplankton: the importance of the eukaryotic component. Limnol Oceanogr 49:168–179

Wyrtki K (1964) Upwelling in the Costa Rica Dome. Fish Bull 63:355–372

Zubkov MV, Mary I, Woodward EMS, Warwick PE, Fuchs BM, Scanlan DJ, Burkill PH (2007) Microbial control of phosphate in the nutrient-depleted North Atlantic subtropical gyre. Environ Microbiol 9:2079–2089

Editorial responsibility: Steven Lohrenz, New Bedford, Massachusetts, USA

Submitted: April 2, 2013; Accepted: May 28, 2014
Proofs received from author(s): August 1, 2014